

# Improving the Transferability of Adversarial Examples with the Adam Optimizer

Heng Yin, Hengwei Zhang, Jindong Wang and Ruiyu Dou

**Abstract:** Convolutional neural networks have outperformed humans in image recognition tasks, but they remain vulnerable to attacks from adversarial examples. Since these data are produced by adding imperceptible noise to normal images, their existence poses potential security threats to deep learning systems. Sophisticated adversarial examples with strong attack performance can also be used as a tool to evaluate the robustness of a model. However, the success rate of adversarial attacks remains to be further improved in black-box environments. Therefore, this study combines an improved Adam gradient descent algorithm with the iterative gradient-based attack method. The resulting Adam Iterative Fast Gradient Method is then used to improve the transferability of adversarial examples. Extensive experiments on ImageNet showed that the proposed method offers a higher attack success rate than existing iterative methods. Our best black-box attack achieved a success rate of 81.9% on a normally trained network and 38.7% on an adversarially trained network.

**Index Terms:** Neural network, Adversarial example, Black-box attack

## 1. Introduction

In image recognition tasks, convolutional neural networks are able to classify images with an accuracy approaching that of humans [1-4]. However, researchers have found that neural networks are also vulnerable to adversarial examples. Szegedy et al. [5] first proposed the concept of adversarial examples: images added with small perturbations, which cause neural network models to output incorrect classifications with high confidence. These adversarial perturbations are often indistinguishable to the human eye (i.e., there is no obvious visual difference between the adversarial examples and the original images).

Adversarial attacks can be categorized into white-box and black-box attacks. A variety of techniques can be used to generate adversarial examples and perform white-box attacks, depending on the model structure and corresponding parameters [6-10]. In addition, adversarial examples are generally transferable as data generated for one model may be able to fool other models. This facilitates black-box attacks, in which the structure and parameters of the model are not available, for various neural networks [11]. Goodfellow et al. [6] suggested that different models learn similar decision boundaries during the same image classification tasks and obtain similar parameters. These

properties make it easier to generalize adversarial examples to different models.

Although adversarial examples are generally transferable, the optimal approach to improving this transferability needs to be examined further. Basic iterative attacks are often more effective than single-step attacks in white-box environments and weaker in black-box environments, due to a balance between attack performance and transferability. In white-box attacks, iterative methods excessively fit specific network parameters, achieving a high success rate but preventing generalization to other models [9]. We propose this to be the result of overfitting, since attack performance for adversarial examples in white-box and black-box environments are similar to the neural network performance on training and test sets.

Unlike white-box attacks, black-box attacks are more consistent with actual attack-defense environments and are primarily performed in one of three ways. 1) Decision-based attacks are conducted using information collected from the network. Although access to model structure and parameters is unavailable, the attacker can generate adversarial examples by executing multiple queries against the model [12-15]. 2) In substitute-model techniques, the attacker can input images into the model to obtain an output label. The substitute model can then be trained to imitate the target model and generate

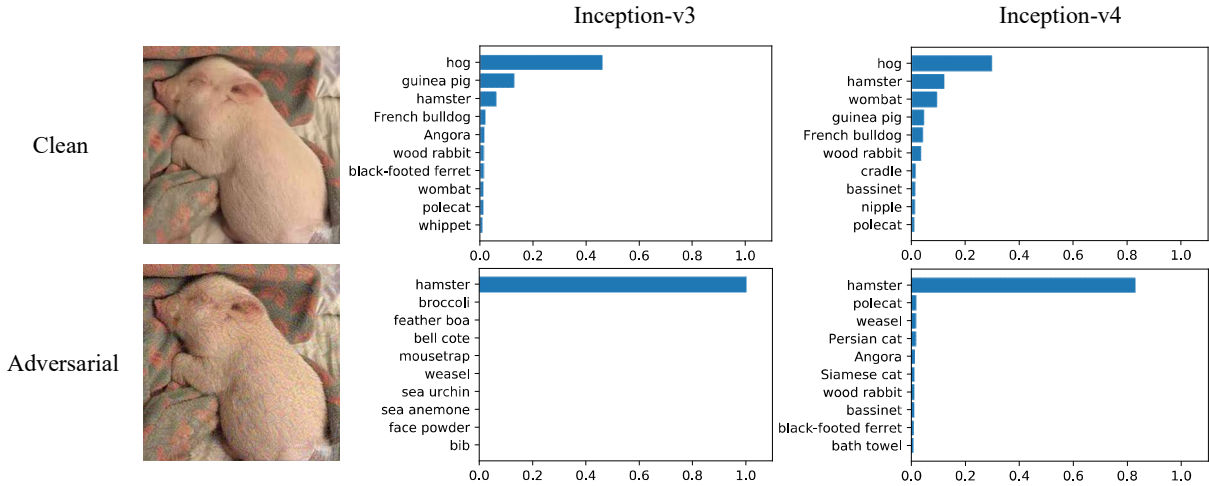


FIGURE 1: Classification of a normal image and corresponding adversarial example by Inc-v3 and Inc-v4. The first row shows the top-10 confidence distributions for a clean image, for which both models provided a correct prediction. The second row shows the top-10 confidence distributions for the adversarial example generated for Inc-v3 by AI-FGM. It is evident that the adversarial example successfully attacked Inc-v3 (white-box) and Inc-v4 (black-box) with high confidence.

adversarial examples [16]. 3) Transferability attacks are conducted by improving the transferability of adversarial examples generated in a white-box setting [8, 9]. The first two black-box attacks require large quantities of model queries, which is impractical in some cases (e.g., online platforms often limit the number of queries). As such, this study investigates black-box attacks using adversarial data with strong transferability. Two types of techniques are often used to improve the transferability of adversarial examples: data augmentation and optimizer-based methods. In this paper we investigate a state-of-the-art optimizer Adam for improving black-box adversarial attacks.

Prior research on adversarial attacks based on gradient has mostly involved iterative algorithms that generate adversarial examples with an invariable step size [6-8]. In this paper, we propose the Adam Iterative Fast Gradient Method (AI-FGM) to improve the transferability of adversarial examples among different models [17]. Compared with other gradient-based methods, the proposed method offers improved attack performance in black-box settings. This approach was tested on multiple networks, including adversarially trained networks, achieving higher attack success rates on black-box models. In addition, we attacked an ensemble of multiple networks, which further improved the transferability of adversarial examples.

## 2. Related Work

### 2.1. Adversarial Attack Methods

Biggio et al. first performed evasion attacks on traditional machine learning models based on MNIST, leading to misclassification of the models [18]. Szegedy et al. found that deep neural networks were vulnerable to adversarial attacks and proposed the L-BFGS method to generate adversarial examples [5]. Goodfellow et al. proposed the Fast

Gradient Sign Method (FGSM) to generate adversarial examples, thereby reducing calculation costs [6]. By extending FGSM, Alexey et al. developed the Iterative Fast Gradient Sign Method (I-FGSM) [7]. Dong et al. proposed the Momentum Iterative Fast Gradient Sign Method (MI-FGSM) to improve the transferability of adversarial data in black-box environments [8]. Moosavidezfooli et al. proposed the DeepFool method, which studies the classifier decision boundary near the input image and attempts to find a direction crossing the boundary [19]. Researchers have also demonstrated that adversarial examples can exist in the physical world and not solely in digital models [7, 20].

### 2.2. Adversarial Defense Methods

Multiple defense mechanisms have been proposed to protect deep learning models from the threat of adversarial examples [21-28]. Among these, adversarial training is the most effective way to improve model robustness [6, 29]. In this process, adversarial examples are generated and added to the training set to participate in the model training procedure. Since normal adversarial training is still vulnerable to adversarial examples, Tramèr et al. proposed ensemble adversarial training to further improve robustness [30]. In this process, adversarial data generated by multiple models are included in the training set for a single model, thereby producing a more robust classifier.

## 3. Methodology

This section provides a detailed introduction to our proposed methodology. Let  $x$  denote an input image and  $y$  denote the corresponding ground-truth label. The term  $\theta$  represents network parameters and  $J(\theta, x, y)$  describes a loss function, typically the cross-entropy loss. The primary objective is to generate an adversarial example  $x^*$  to fool the model by maximizing  $J(\theta, x, y)$ , such that the prediction label

$y^{pre} \neq y$ . In this paper, we used an  $L_\infty$  norm bound to limit adversarial perturbations, such that  $\|x^* - x\|_\infty \leq \varepsilon$ , where  $\varepsilon$  is the size of the perturbation. The generation of adversarial examples can therefore be converted into the following optimization problem:

$$\arg \max_{x^*} J(\theta, x^*, y), \quad s.t. \|x^* - x\|_\infty \leq \varepsilon \quad (1)$$

### 3.1. Attack Methods Based on a Gradient

This section provides a brief introduction to several techniques used to solve the optimization problem described above.

- **Fast Gradient Sign Method (FGSM) [6]:** This is one of the simplest techniques, which seeks adversarial examples in the direction of the gradient of the loss function with respect to the input image  $x$ . The method can be expressed as:

$$x^* = x + \varepsilon \cdot \text{sign}(\nabla_x J(\theta, x, y)) \quad (2)$$

- **Iterative Fast Gradient Sign Method (I-FGSM) [7]:** This algorithm is an iterative version of FGSM. The approach involves dividing the FGSM gradient operation into multiple steps that can be expressed as follows:

$$x_0^* = x, \quad x_{i+1}^* = x_i^* + \alpha \cdot \text{sign}(\nabla_x J(\theta, x_i^*, y)), \quad (3)$$

$$x_{i+1}^* = \text{Clip}(x_{i+1}^*, x - \varepsilon, x + \varepsilon), \quad (4)$$

where  $\alpha$  is the step size of each iteration and  $\alpha = \varepsilon / T$ , in which  $T$  is the number of iterations. The *Clip* function was included to limit the adversarial example  $x^*$  within the  $\varepsilon$  neighborhood of the original image  $x$  and satisfy the  $L_\infty$  norm constraint. I-FGSM is more effective than FGSM in white-box environments, but less effective in black-box environments. In other words, I-FGSM exhibits poor transferability.

- **Momentum Iterative Fast Gradient Sign Method (MI-FGSM) [8]:** In this method, a momentum term is applied to the iterative process to escape from poor local maxima. This produces adversarial examples with more transferability, which can be expressed as [8]:

$$x_0^* = x, \quad g_0 = 0, \quad g_{i+1} = \mu \cdot g_i + \frac{\nabla_x J(\theta, x_i^*, y)}{\|\nabla_x J(\theta, x_i^*, y)\|_1}, \quad (5)$$

$$x_{i+1}^* = x_i^* + \alpha \cdot \text{sign}(g_{i+1}), \quad (6)$$

$$x_{i+1}^* = \text{Clip}(x_{i+1}^*, x - \varepsilon, x + \varepsilon), \quad (7)$$

where  $\mu$  is the decay factor of the momentum term and  $g_i$  is the weighted accumulation of gradients in the first  $i$  rounds of iterations.

### 3.2. Adam Iterative Fast Gradient Method

Adam [17] is an optimization algorithm combining

momentum [31] and RMSProp [32]. In the iteration process, Adam accumulates not only the gradients of the loss function with respect to the input image, but also the square of the gradients. This is done to accelerate loss function ascent in dimensions with small gradients. In addition, Adam uses a decreasing step size in each iteration to achieve better convergence.

In contrast, both I-FGSM and MI-FGSM adopt a constant step size. In the latter stages of the algorithm, oscillations occur near the local maximum, which do not converge well. To solve this problem, we have improved the Adam algorithm by normalizing the step size sequence (defined in Eq. (13)) and have applied it to the iterative gradient method. The resulting Adam Iterative Fast Gradient Method (AI-FGM), proposed in this study, is summarized in Algorithm 1.

Specifically, the gradient  $\nabla_x J(\theta, x_i^*, y)$  in each iteration is normalized by its own  $L_1$  distance, defined in Eq. (9), because the scale of these gradients differs widely in each iteration [8]. Similar to MI-FGSM,  $m_t$  accumulates

---

#### Algorithm 1 Adam Iterative Fast Gradient Method

---

**Input:** A convolutional neural network  $f$  and the corresponding cross-entropy loss function  $J(\theta, x, y)$ ; an original image  $x$  and the corresponding ground-truth label  $y$ ; the number of iterations  $T$ ; the iteration time step  $t$ ; the dimension of the input image  $N$ ; the size of the perturbation  $\varepsilon$ ; Adam decay factors  $\beta_1$  and  $\beta_2$ ; and a denominator stability factor  $\delta$ .

**Output:** An adversarial example  $x^*$ , such that  $\|x - x^*\|_\infty \leq \varepsilon$ .

1.  $m_0 = 0, v_0 = 0, x_0^* = x$ , and  $t = 0$ ;

2.  $\alpha = \varepsilon \cdot \sqrt{N}$ ; (8)

3. **while**  $t < T$  **do:**

4.  $g_t = \frac{\nabla_x J(\theta, x_t^*, y)}{\|\nabla_x J(\theta, x_t^*, y)\|_1}$ ; (9)

5.  $m_{t+1} = \beta_1 m_t + (1 - \beta_1) g_t$ ; (10)

6.  $v_{t+1} = \beta_2 \cdot v_t + (1 - \beta_2) \cdot g_t^2$ ; (11)

7.  $s_{t+1} = \frac{m_{t+1}}{\delta + \sqrt{v_{t+1}}}$ ; (12)

8.  $\alpha_t = \alpha \cdot \frac{\sqrt{1 - \beta_2^{t+1}}}{1 - \beta_1^{t+1}} \bigg/ \sum_{i=0}^{T-1} \frac{\sqrt{1 - \beta_2^{i+1}}}{1 - \beta_1^{i+1}}$ ; (13)

9.  $x_{t+1}^* = x_t^* + \alpha_t \cdot \frac{s_{t+1}}{\|s_{t+1}\|_2}$ ; (14)

10.  $x_{t+1}^* = \text{Clip}(x_{t+1}^*, x - \varepsilon, x + \varepsilon)$ ; (15)

11.  $t = t + 1$ ;

12. **end while**

13. **return**  $x^* = x_T^*$ .

---

gradients of the first  $t$  iterations with a decay factor  $\beta_1$ , defined in Eq. (10). The result can be considered the first momentum. The term  $v_t$  represents the second momentum, which accumulates the squares of gradients for the first  $t$  iterations with a decay factor  $\beta_2$ , defined in Eq. (11). It should be noted that  $g_t^2$  denotes an elementwise square  $g_t \odot g_t$ , where  $\odot$  represents the Hadamard product [31]. The terms  $\beta_1$  and  $\beta_2$  are typically defined in the range (0,1). The update direction of input  $x$  is defined in Eq. (12), where the stability coefficient  $\delta$  was set to avoid a zero in the denominator. The  $s_t$  term is advantageous as it prompts  $x$  to escape from local maxima and accelerates the updating of  $x$  in dimensions with small gradients.

Learning rate decay is often used in the training of neural networks. In this study, the step size used in the Adam optimizer was continually reduced to help improve the convergence of the algorithm. If  $\beta_1$  and  $\beta_2$  are set appropriately, the value of  $\sqrt{1-\beta_2^t}/(1-\beta_1^t)$  will decrease as  $t$  increases. Thus, a decreasing sequence can be generated when  $t$  ranges from 0 to  $T-1$ . The sequence can then be normalized to obtain the weight of step sizes in each iteration, relative to the total step size  $\alpha$ . This can be used to acquire a set of exponential decay step sizes controlled by  $\beta_1$  and  $\beta_2$ , as defined in Eq. (13).

Existing techniques typically use the sign function to satisfy the  $L_\infty$  norm limitation. However, if the sign function was applied in Eq. (14), the update direction in our method would be equivalent to that of MI-FGSM. As such, we constrain adversarial examples within the  $L_\infty$  norm bound by the *Clip* function and apply the step size and update direction within the corresponding  $L_2$  norm bound, defined in Eqs. (14) and (15). The relationship between the  $L_\infty$  norm bound ( $\varepsilon$ ) and the  $L_2$  norm bound ( $\alpha$ ) is defined in Eq. (8), where  $N$  represents the dimension of the input image  $x$ .

### 3.3. Attacking an Ensemble of Networks

The proposed method was also used to attack an ensemble of networks. If an adversarial example poses a threat to multiple networks, it is far more likely to transfer to other models [11]. We followed the ensemble strategy proposed by Dong et al., in which multiple models are attacked by fusing network logits [8]. Specifically, to attack an ensemble of  $K$  models, logits were fused as follows:

$$l(x) = \sum_{k=1}^K \omega_k l_k(x), \quad (16)$$

Where  $l_k(x)$  is the logit output of the  $k^{\text{th}}$  model,  $\omega_k$  is the ensemble weight ( $\omega_k \geq 0$ ), and  $\sum_{k=1}^K \omega_k = 1$ .

## 4. Experiment

Extensive validation experiments were conducted to demonstrate the effectiveness of the proposed methodology. Experimental settings are provided in Sec. 4.1. The results of attacking a single network are discussed in Sec. 4.2, along with discussions of some parameters that influenced the results. Finally, Sec. 4.3 details an attack on an ensemble of models.

### 4.1. Experimental Setup

- Dataset:** If the original images cannot be classified correctly by the network, it is meaningless to generate adversarial examples based on these data. As such, we selected 1000 images belonging to the 1000 categories from ImageNet validation set, all of which could be classified correctly by the tested networks. All images were scaled to  $299 \times 299 \times 3$ . As such,  $N = 299 \times 299 \times 3$  in Sec. 3.2.

TABLE 1: Success rates (%) for all seven networks included in the study. The diagonal blocks indicate white-box attacks and the off-diagonal blocks indicate black-box attacks.

	Attack	Inc-v3	Inc-v4	IncRes-v2	Res-152	Inc-v3 <sub>ens3</sub>	Inc-v3 <sub>ens4</sub>	IncRes-v2 <sub>ens</sub>
Inc-v3	FGSM	71.9	28.1	26.3	28.7	11.6	10.9	5.0
	I-FGSM	<b>100.0</b>	22.4	20.5	17.5	7.4	7.5	4.0
	MI-FGSM	<b>100.0</b>	45.0	44.3	34.3	13.3	13.1	6.3
	AI-FGM	<b>100.0</b>	<b>52.4</b>	<b>50.2</b>	<b>42.6</b>	<b>18.5</b>	<b>17.3</b>	<b>8.7</b>
Inc-v4	FGSM	32.8	61.1	26.4	28.9	13.3	11.9	6.3
	I-FGSM	37.7	<b>99.9</b>	26.5	21.8	8.6	7.9	5.0
	MI-FGSM	61.0	<b>99.9</b>	50.6	43.1	16.8	14.8	8.5
	AI-FGM	<b>68.4</b>	99.8	<b>56.1</b>	<b>48.7</b>	<b>22.7</b>	<b>18.8</b>	<b>10.3</b>
IncRes-v2	FGSM	33.0	28.4	55.3	28.1	13.4	12.1	7.2
	I-FGSM	37.5	31.4	<b>99.6</b>	25.8	9.0	7.6	4.9
	MI-FGSM	64.6	58.7	<b>99.6</b>	47.9	25.3	17.3	13.3
	AI-FGM	<b>69.1</b>	<b>62.5</b>	<b>99.6</b>	<b>52.8</b>	<b>28.3</b>	<b>24.1</b>	<b>18.7</b>
Res-152	FGSM	34.2	29.9	27.5	78.7	13.8	11.5	7.1
	I-FGSM	27.6	23.5	21.2	98.2	9.2	8.0	5.5
	MI-FGSM	50.4	45.1	42.8	98.2	20.3	18.2	10.7
	AI-FGM	<b>57.2</b>	<b>51.3</b>	<b>47.5</b>	<b>98.4</b>	<b>25.2</b>	<b>22.3</b>	<b>14.0</b>

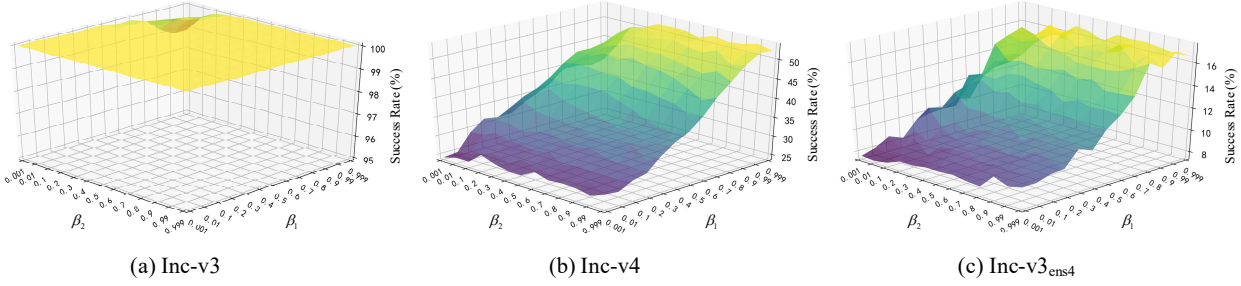


FIGURE 2: Success rates (%) of adversarial examples generated for Inc-v3 with AI-FGM, applied to Inc-v3 (white-box), Inc-v4 (black-box and normally trained), and Inc-v3<sub>ens4</sub> (black-box and adversarially trained) with  $\beta_1$  and  $\beta_2$  in the range (0,1).

- Networks:** Seven different models were studied, four of which were normally trained networks (i.e., Inception-v3 (Inc-v3) [33], Inception-v4 (Inc-v4) [34], Inception-Resnet-v2 (IncRes-v2) [34], and Resnet-v2-152 (Res-152) [35]). The other three models were adversarially trained networks (i.e., ens3-adv-Inception-v3 (Inc-v3<sub>ens3</sub>), ens4-adv-Inception-v3 (Inc-v3<sub>ens4</sub>), and ens-adv-Inception-ResNet-v2 (IncRes-v2<sub>ens</sub>) [30]).
- Other details:** The proposed method was compared to the other methods discussed in Sec. 3.1. All the experiments described in this paper were based on the  $L_\infty$  norm. Thus, the momentum decay factor  $\mu$  in Eq. (5) was 1.0 and the stability coefficient  $\delta$  in Eq. (12) was  $10^{-8}$ , as suggested in [17].

#### 4.2. Attacking a Single Network

We first performed adversarial attacks on a single network with FGSM, I-FGSM, MI-FGSM, and AI-FGM. And the adversarial examples were generated on four normally trained networks and tested on all seven networks. The results are shown in Table 1, where the success rates are misclassification rates for the corresponding models, with adversarial examples used as input. The decay factors  $\beta_1$  and  $\beta_2$  in AI-FGM were set to 0.99 and 0.999, respectively. The maximum perturbation  $\varepsilon$  was 16. The number of iterations  $T$  for I-FGSM, MI-FGSM, and AI-FGM was 10. These three methods are hereafter referred to as “iterative methods” without ambiguity. The effects of these parameter choices are discussed further in this section.

It is evident from Table 1 that all three iterative methods attacked a white-box model with a near 100% success rate. AI-FGM performed better than the other three methods on all black-box models. For example, for adversarial examples generated on Inc-v3, AI-FGM had a success rate of 52.4% on Inc-v4, while MI-FGSM, I-FGSM, and FGSM reached 45.0%, 22.4%, and 28.1%, demonstrating the effectiveness of the proposed model. An original image and the corresponding adversarial example generated for Inc-v3 by AI-FGM are shown in Fig. 1.

##### 4.2.1. Decay Factors

The terms  $\beta_1$  and  $\beta_2$  control not only the decay amplitude of the step sizes, but also the accumulation intensity of

gradients for  $m_t$  and  $v_t$ . As such, they have a direct impact on attack success rates. We applied a grid-search method to identify an optimal set of  $\beta_1$  and  $\beta_2$  values. In the experiments, the maximum perturbation  $\varepsilon$  was set to 16 and the number of iterations  $T$  was set to 10. The values of  $\beta_1$  and  $\beta_2$  ranged from 0 to 1. It should be noted that not only did we choose the values of  $\beta_1$  and  $\beta_2$  uniformly from 0.1 to 0.9, but we also choose values close to 0 and 1, as shown in Fig. 2. This was done to provide a more comprehensive study on the effects of decay factors, as we propose the relationship between the success rate and the decay factors may be nonlinear. Adversarial examples were then generated on Inc-v3 with AI-FGM and used to perform attacks on Inc-v3, Inc-v4, and Inc-v3<sub>ens4</sub>. It is evident from the figure that regardless of the values of  $\beta_1$  and  $\beta_2$ , attack success rates were always near 100% in white-box environments. Attack success rates were more sensitive to  $\beta_1$  for black-box models, regardless of whether networks were normally or adversarially trained. Success rates were maximized when both  $\beta_1$  and  $\beta_2$  were close to 1.

##### 4.2.2. The Number of Iterations

The effect of iteration quantities on success rates was studied by performing attacks using iterative methods. The maximum perturbation  $\varepsilon$  was set to 16 and the decay factors  $\beta_1$  and  $\beta_2$  were set to 0.99 and 0.999, respectively. The number of iterations  $T$  ranged from 1 to 20. Adversarial examples generated on Inc-v3 with I-FGSM, MI-FGSM, and AI-FGM were then used to attack Inc-v3 and Inc-v4, as shown in Fig. 3.

From the figure, we observe the success rates of black-box attacks for several iterative methods decreased with increasing iteration quantities. However, AI-FGM always outperformed I-FGSM and MI-FGSM for a given value of  $T$ .

##### 4.2.3. Perturbation Size

The effect of adversarial perturbation size on attack success rates was studied by setting the number of iterations  $T$  to 10, with decay factors of 0.99 and 0.999. The size of perturbations  $\varepsilon$  ranged from 1 to 30. Adversarial examples generated on Inc-v3 with I-FGSM, MI-FGSM, and AI-FGM were used to attack Inc-v3 and Inc-v4, as shown in Fig. 4.

It is evident from the figure that attack success rates can

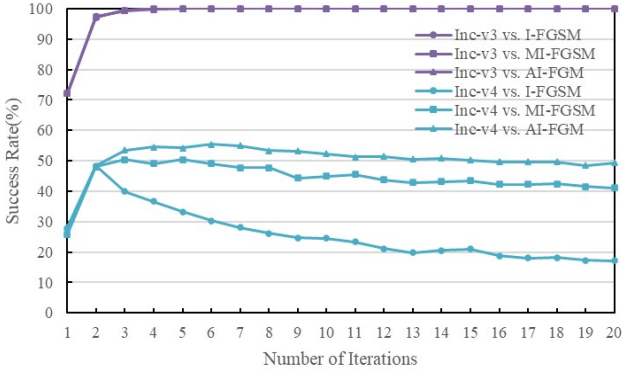


FIGURE 3: Success rates (%) of adversarial examples generated for Inc-v3 with I-FGSM, MI-FGSM, and AI-FGM, applied to Inc-v3 (white-box) and Inc-v4 (black-box) with  $T$  ranging from 1 to 20. It should be noted that the curves of Inc-v3 vs. I-FGSM, Inc-v3 vs. MI-FGSM, and Inc-v3 vs. AI-FGM overlap.

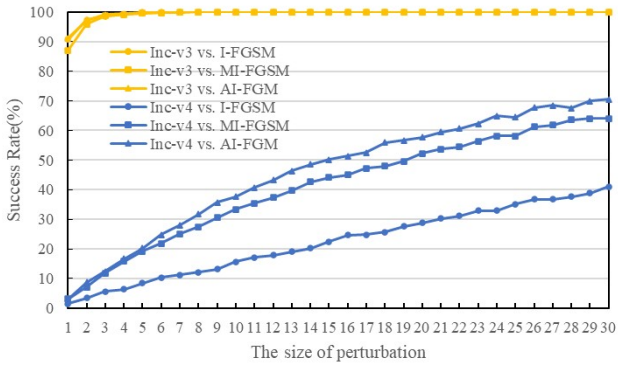


FIGURE 4: Success rates (%) of adversarial examples generated for Inc-v3 with I-FGSM, MI-FGSM, and AI-FGM, applied to Inc-v3 (white-box) and Inc-v4 (black-box) with  $\epsilon$  ranging from 1 to 30. It should be noted that the curves of Inc-v3 vs. I-FGSM, Inc-v3 vs. MI-FGSM, and Inc-v3 vs. AI-FGM overlap.

reach 100% in white-box environments. Success rates for black-box models increased steadily with increasing values of  $\epsilon$ . AI-FGM always outperformed I-FGSM and MI-FGSM for a given value of  $\epsilon$ . In other words, AI-FGM can achieve comparable black-box attack success rates with smaller perturbations.

TABLE 2: Success rates (%) for ensemble attacks. The “-” symbol indicates the name of the hold-out network. Adversarial examples were generated on the ensemble of the other six networks. The first row shows success rates for the ensemble networks (white-box) and the second row shows success rates for the hold-out network (black-box).

	Attack	-Inc-v3	-Inc-v4	-IncRes-v2	-Res-152	-Inc-v3 <sub>ens3</sub>	-Inc-v3 <sub>ens4</sub>	-IncRes-v2 <sub>ens</sub>
Ensemble	FGSM	22.5	21.2	21.7	22.5	35.7	33.3	37.9
	I-FGSM	98.4	98.3	99.1	97.9	98.1	98.2	96.2
	MI-FGSM	98.8	98.6	<b>99.5</b>	97.8	98.5	98.5	96.9
	AI-FGM	<b>99.4</b>	<b>99.2</b>	99.3	<b>98.0</b>	<b>99.4</b>	<b>99.2</b>	<b>99.4</b>
Hold-out	FGSM	44.0	38.3	40.2	31.3	11.7	12.6	5.6
	I-FGSM	54.3	48.2	48.9	41.1	17.3	18.6	10.7
	MI-FGSM	75.3	69.8	67.3	62.6	25.4	31.3	19.2
	AI-FGM	<b>81.9</b>	<b>76.7</b>	<b>73.1</b>	<b>68.5</b>	<b>32.9</b>	<b>38.7</b>	<b>24.8</b>

### 4.3. Attacking an Ensemble of Networks

The experimental results presented above suggest AI-FGM can increase the transferability of adversarial examples. In addition, the success rate of black-box attacks can be further improved by attacking an ensemble of networks. As discussed in Sec. 3.3, multiple models were attacked by fusing network logits. In the experiment, all seven networks described in Sec. 4.1 were used, and we generate adversarial examples on the ensemble of six networks with FGSM, I-FGSM, MI-FGSM, and AI-FGM. Attacks were then performed on ensemble networks and a hold-out network. Decay factors were set to 0.99 and 0.999, the number of iterations was 10, the maximum perturbation was 16, and each network had an equal ensemble weight of  $\omega_k = 1/6$ . The corresponding results are shown in Table 2, where it is evident that AI-FGM achieved high success rates in white-box environments and was also more effective than the other three methods in black-box settings. For example, when Inc-v3 was used as the hold-out network, AI-FGM reached an attack success rate of 81.9% for Inc-v3. In contrast, success rates for MI-FGSM, I-FGSM, and FGSM were 75.3%, 54.3%, and 44.0%, respectively.

These results also revealed an interesting feature of the FGSM algorithm. Unlike with iterative methods, when normally trained networks (the first 4 columns in Table 2) were attacked by adversarial examples generated with FGSM, attack success rates for hold-out networks were higher than those of ensemble networks. In other words, the black-box success rates were higher than white-box success rates. This is counterintuitive and is worth studying in more detail.

## 5. Discussion

It is commonly acknowledged that the training of neural network models is similar to the generation of adversarial examples, especially for gradient-based generation methods. As such, techniques used in the training of neural networks, to improve model generalizability, can also be used to improve the transferability of adversarial examples. Since the

Adam optimizer is often used in the training of neural networks, to improve convergence and achieve better performance on test sets, a second momentum term and decay step size were included in the AI-FGM algorithm. This was done to improve the transferability of adversarial examples. Furthermore, we suggest that other techniques (e.g., data augmentation) could be used to further improve the performance of adversarial examples in black-box environments.

## 6. Conclusion

In this study, we proposed the Adam Iterative Fast Gradient Method to improve the transferability of adversarial examples. Specifically, the Adam algorithm was modified to increase its suitability for the generation of adversarial examples. The resulting method improved both the iteration update direction and step size. The effectiveness of the proposed method was verified by an extensive series of experiments with ImageNet. Compared with previous gradient-based adversarial example generation techniques, our method improved attack success rates in black-box environments. In addition, an attack on an ensemble of networks was performed to further improve the transferability of adversarial examples. We suggest the proposed method could be used as a reference for other iterative gradient-based methods. For example, data augmentation could be combined with AI-FGM to achieve better attack performance.

## References

- [1] A. Krizhevsky, I. Sutskever, and G. E. Hinton, "ImageNet classification with deep convolutional neural networks," *Commun. ACM*, vol. 60, no. 6, pp. 84–90, May 2017.
- [2] K. Simonyan and A. Zisserman, "Very deep convolutional networks for large-scale image recognition," 2014, arXiv: 1409.1556. [Online]. Available: <http://arxiv.org/abs/1409.1556>.
- [3] C. Szegedy *et al.*, "Going deeper with convolutions," in *Proc. IEEE Conf. Comput. Vision Pattern Recognit. (CVPR)*, Boston, MA, USA, 2015, pp. 1–9.
- [4] K. He, X. Zhang, S. Ren, and J. Sun, "Deep Residual Learning for Image Recognition," in *Proc. IEEE Conf. Comput. Vision Pattern Recognit. (CVPR)*, Las Vegas, NV, USA, 2016, pp. 770–778.
- [5] C. Szegedy *et al.*, "Intriguing properties of neural networks," 2013, arXiv: 1312.6199. [Online]. Available: <https://arxiv.org/abs/1312.6199>.
- [6] I. J. Goodfellow, J. Shlens, and C. Szegedy, "Explaining and harnessing adversarial examples," 2014, arXiv: 1412.6572. [Online]. Available: <https://arxiv.org/abs/1412.6572>.
- [7] A. Kurakin, I. Goodfellow, and S. Bengio, "Adversarial examples in the physical world," 2016, arXiv: 1607.02533. [Online]. Available: <https://arxiv.org/abs/1607.02533>.
- [8] Y. Dong *et al.*, "Boosting adversarial attacks with momentum," in *Proc. IEEE/CVF Conf. Comput. Vision Pattern Recognit.*, Salt Lake City, UT, USA, 2018, pp. 9185–9193.
- [9] C. Xie *et al.*, "Improving transferability of adversarial examples with input diversity," in *Proc. IEEE Conf. Comput. Vision Pattern Recognit. (CVPR)*, Long Beach, CA, USA, 2019, pp. 2725–2734.
- [10] N. Carlini and D. Wagner, "Towards evaluating the robustness of neural networks," in *Proc. IEEE Symp. Secur. Privacy*, San Jose, CA, USA, 2017, pp. 39–57.
- [11] Y. Liu, X. Chen, C. Liu, and D. Song, "Delving into transferable adversarial examples and black-box attacks," 2016, arXiv: 1611.02770. [Online]. Available: <https://arxiv.org/abs/1611.02770>.
- [12] A. I. Ilyas, L. Engstrom, A. Athalye, and J. Lin, "Black-box adversarial attacks with limited queries and information," 2018, arXiv: 1804.08598. [Online]. Available: <https://arxiv.org/abs/1804.08598>.
- [13] D. Wierstra, T. Schaul, T. Glasmachers, Y. Sun, J. Peters, and J. Schmidhuber, "Natural evolution strategies," *J. Mach. Learn. Res.*, vol. 15, no. 1, pp. 949–980, 2014.
- [14] M. Alzantot, Y. Sharma, S. Chakraborty, H. Zhang, C. J. Hsieh, and M. B. Srivastava, "GenAttack: practical black-box attacks with gradient-free optimization," in *Proc. Genetic Evol. Comput. Conf. (GECCO '19)*, New York, NY, USA, 2019, pp. 1111–1119.
- [15] W. Brendel, J. Rauber, and M. Bethge, "Decision-based adversarial attacks: Reliable attacks against black-box machine learning models," 2017, arXiv: 1712.04248. [Online]. Available: <https://arxiv.org/abs/1712.04248>.
- [16] N. Papernot, P. McDaniel, I. Goodfellow, S. Jha, Z. B. Celik, and A. Swami, "Practical black-box attacks against machine learning," in *Proc. Asia Conf. Comput. Commun. Secur.*, Abu Dhabi, United Arab Emirates, 2017, pp. 506–519.
- [17] D. P. Kingma and J. Ba, "Adam: A method for stochastic optimization," 2014, arXiv: 1412.6980. [Online]. Available: <https://arxiv.org/abs/1412.6980>.
- [18] B. Biggio *et al.*, "Evasion attacks against machine learning at test time," in *Proc. Mach. Learn. Knowl. Discovery Databases*, Berlin, Heidelberg, 2013, pp. 3876–402.
- [19] S. Moosavi-Dezfooli, A. Fawzi, and P. Frossard, "Deepfool: A simple and accurate method to fool deep neural networks," in *Proc. IEEE Conf. Comput. Vision Pattern Recognit. (CVPR)*, Las Vegas, NV, USA, 2016, pp. 2574–2582.
- [20] K. Eykholt *et al.*, "Robust physical-world attacks on deep learning visual classification," in *Proc. IEEE/CVF Conf. Comput. Vision Pattern Recognit.*, Salt Lake City, UT, USA,

- 2018, pp. 1625–1634.
- [21] A. Madry, A. Makelov, L. Schmidt, D. Tsipras, and A. Vladu, "Towards deep learning models resistant to adversarial attacks," 2018, arXiv: 1706.06083. [Online]. Available: <https://arxiv.org/abs/1706.06083>.
- [22] N. Papernot, P. McDaniel, X. Wu, S. Jha, and A. Swami, "Distillation as a defense to adversarial perturbations against deep neural networks," in *Proc. IEEE Symp. Secur. Privacy*, San Jose, CA, USA, 2016, pp. 582–597.
- [23] J. Buckman, A. Roy, C. Raffel, and I. Goodfellow, "Thermometer encoding: One hot way to resist adversarial examples," in *Proc. Int. Conf. Learn. Representations*, Vancouver, BC, Canada, 2018.
- [24] C. Guo, M. Rana, M. Cissé, and L. V. D. Maaten, "Countering adversarial images using input transformations," 2017, arXiv: 1711.00117. [Online]. Available: <https://arxiv.org/abs/1711.00117>.
- [25] P. Samangouei, M. Kabkab, and R. Chellappa, "Defense-gan: Protecting classifiers against adversarial attacks using generative models," 2018, arXiv: 1805.06605. [Online]. Available: <https://arxiv.org/abs/1805.06605>.
- [26] A. Levine and S. Feizi, "Wasserstein smoothing: Certified robustness against wasserstein adversarial attacks," in *Proc. Int. Conf. Artif. Intell. Statist. (AISTATS)* Palermo, Italy, 2020.
- [27] C. Mao *et al.*, "Multitask Learning Strengthens Adversarial Robustness," 2020, arXiv: 2007.07236. [Online]. Available: <https://arxiv.org/abs/2007.07236>.
- [28] J. M. Cohen, E. Rosenfeld, and J. Z. Kolter, "Certified adversarial robustness via randomized smoothing," 2019, arXiv: 1902.02918. [Online]. Available: <https://arxiv.org/abs/1902.02918>.
- [29] A. Kurakin, I. Goodfellow, and S. Bengio, "Adversarial machine learning at scale," 2016, arXiv: 1611.01236. [Online]. Available: <https://arxiv.org/abs/1611.01236>.
- [30] F. Tramèr, A. Kurakin, N. Papernot, D. Boneh, and P. McDaniel, "Ensemble adversarial training: Attacks and defenses," 2017, arXiv: 1705.07204. [Online]. Available: <https://arxiv.org/abs/1705.07204>.
- [31] I. Sutskever, J. Martens, G. Dahl, and G. Hinton, "On the importance of initialization and momentum in deep learning," in *Proc. Int. Conf. Mach. Learn.*, Atlanta, GA, USA, 2013, pp. 1139–1147.
- [32] T. Tieleman and G. Hinton, "Lecture 6.5 - RMSProp, coursera: Neural networks for machine learning," *Tech. Rep.*, 2012.
- [33] C. Szegedy, V. Vanhoucke, S. Ioffe, J. Shlens, and Z. Wojna, "Rethinking the inception architecture for computer vision," in *Proc. IEEE Conf. Comput. Vision Pattern Recognit. (CVPR)*, Las Vegas, NV, USA, 2016, pp. 2818–2826.
- [34] C. Szegedy, S. Ioffe, V. Vanhoucke, and A. A. Alemi, "Inception-v4, inception-ResNet and the impact of residual connections on learning," presented at the AAAI Conf. Artif. Intell., San Francisco, California, USA, 2017.
- [35] K. He, X. Zhang, S. Ren, and J. Sun, "Identity mappings in deep residual networks," in *Proc. Comput. Vision – ECCV 2016*, Cham, 2016, pp. 630–645.